NUCLEON STRUCTURE AT SMALL x: RECENT RESULTS FROM HERA

M. Kuhlen

Max-Planck-Institut für Physik, Werner-Heisenberg-Institut
Föhringer Ring 6, D-80805 München, Germany
E-mail: kuhlen@.desy.de

Measurements of structure functions and of the hadronic final state in deep inelastic scattering at HERA are presented. The results comprise the extraction of parton densities, measurements of the strong coupling, and the search for novel QCD effects in the new kinematic regime at HERA.

1. Introduction

1.1. Overview

Data from the electron[1]-proton collider HERA at DESY in Hamburg provide new insights into the structure of the proton. Electrons with $E_e = 27$ GeV collide with protons of $E_p = 820$ GeV , giving rise to a total ep centre of mass (CM) energy of $\sqrt{s} = \sqrt{4E_eE_p} \approx 300$ GeV . The high energy allows to probe the proton in hitherto unexplored kinematic regions. Two complementary sources of information can be identified: the measurement of the inclusive $ep \to e'H$ deep inelastic scattering (DIS) cross section, where H stands for any hadronic system, and measurements of the hadronic system H itself. The cross section measurements are expressed in structure functions, which in turn can be interpreted in terms of parton (i.e. quark and gluon) densities in the proton. In simple words, how often the probe hits something inside the proton determines its content.

The hadronic final state H on the other hand can be viewed as the materialization of the quantum fluctuations inside the proton, allowing in principle a more direct, but due to confinement also a more complicated, access to the dynamics inside the proton. In addition, due to the large phase space, the hadronic final state serves as a QCD laboratory with tunable initial kinematic conditions.

1.2. Kinematics

The kinematics of the basic scattering process in Fig.1 can be characterized by any set of two Lorentz-invariants out of Q^2, x, y, W, which are built from the 4-momentum transfer $q = k - k'$ mediated by the virtual boson, and by the 4-momentum p of the incoming proton. These are:

$Q^2 = -q^2$, which gives the resolving power of the probe with wavelength $\lambda = 1/Q$ (we set $\hbar = c = 1$);

$x = Q^2/(2pq)$, the Bjorken scaling variable, which can be interpreted as the momentum fraction of the proton which is carried by the struck quark;

$y = Q^2/(xs)$, the transferred energy fraction from the electron to the proton in the proton rest frame; and

$W^2 = Q^2(1-x)/x + m_p^2 \approx sy - Q^2$, the invariant mass squared of the hadronic system H.

The large CM energy give access to kinematic regions both at very small x and at large Q^2 (Fig.2). The HERA data cover roughly $Q^2 = 0.2 - 10^4$ GeV^2, $x = 10^{-5} - 10^{-1}$ and $W = 40 - 300$ GeV .

1.3. Detectors

Two large multi-purpose colliding beam detectors, H1 and ZEUS, are installed around the collision regions (Fig.1b). They consist mainly of inner tracking devices, followed by calorimetry and outer muon detection systems. They allow to measure both the scattered electron and the hadronic final state, apart from the proton remnant, which largely escapes detection in the beam pipe. The scattered electron serves as a tag of DIS events, distinguishing them from an otherwise overwhelming background from photoproduction (quasi real photons with $Q^2 \approx 0$) and beam-gas reactions. The kinematics can be determined either from the electron alone, or from the measured hadronic system alone, or from a combination of both, permitting important systematic cross checks.

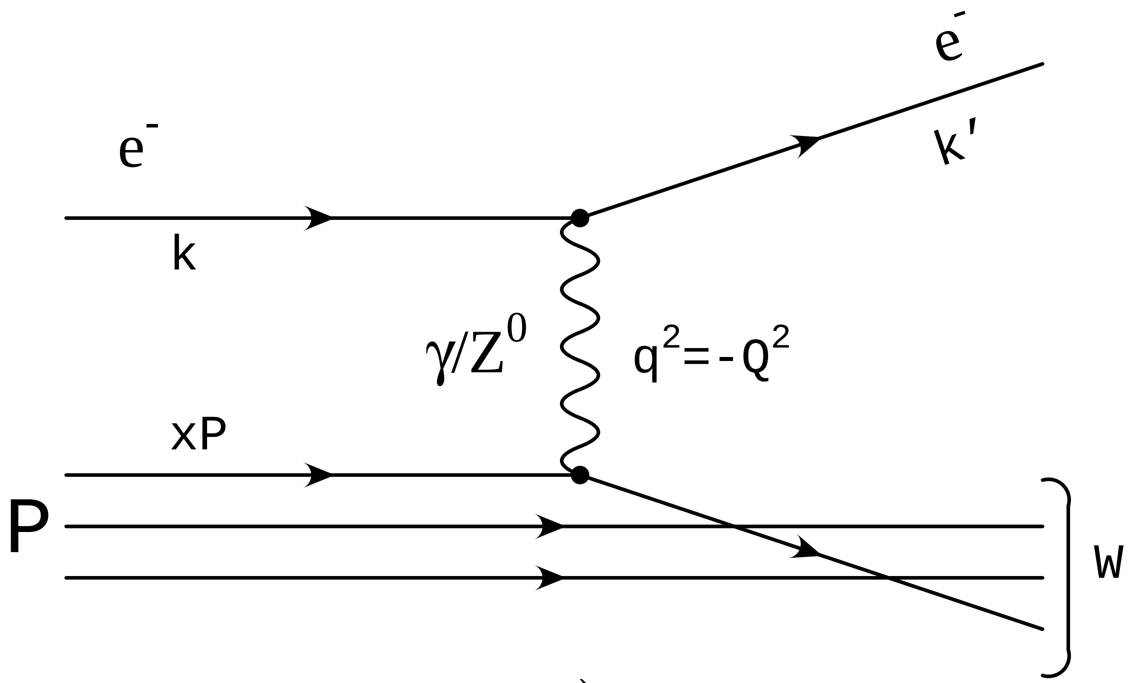

a)

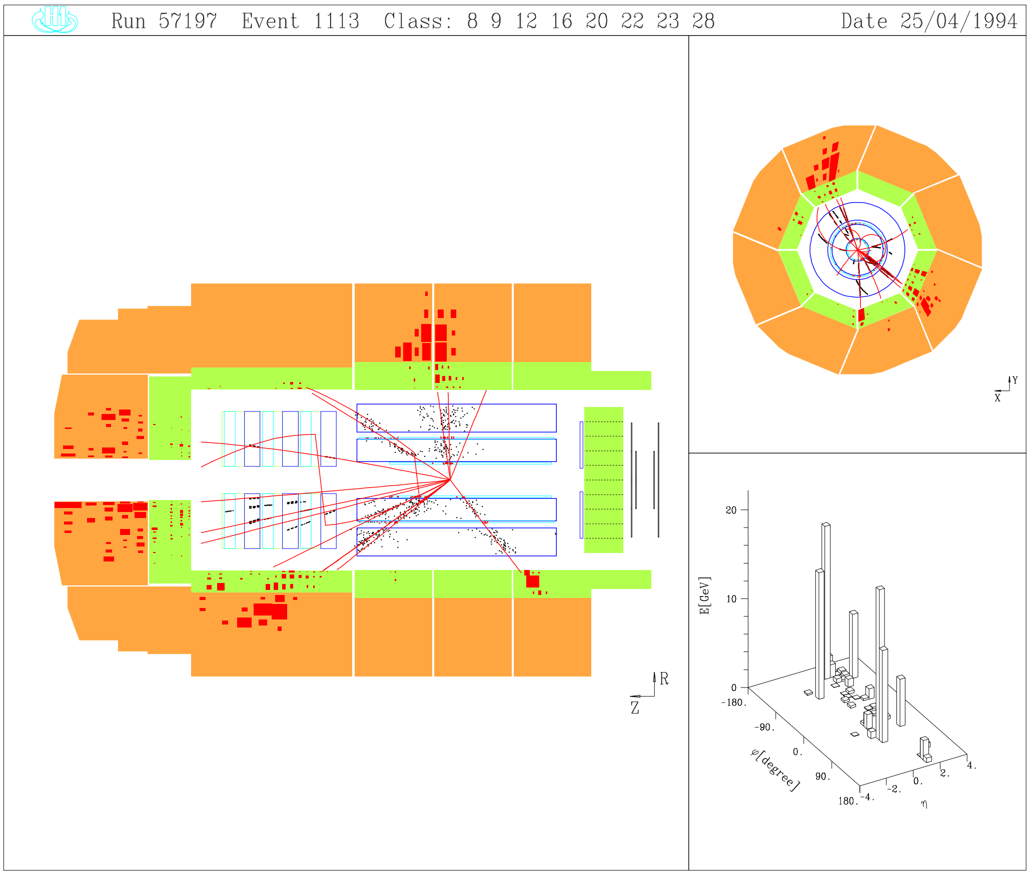

b)

Figure 1: **a)** Basic diagram for DIS in $O(\alpha_s^0)$ (quark parton model - QPM). **b)** As an example, a DIS event with the scattered electron and two well separated jets detected in the H1 detector is shown. The proton remnant leaves mostly undetected in the $+z$ direction.

2. Structure functions

The fundamental measurement in DIS concerns the cross section for $ep \to e'H$ as a function of the kinematic variables. The quark parton model (QPM) offers a physical picture: the scattering takes place via a virtual photon which is radiated off the scattering electron, and which couples to a pointlike constituent inside the proton, that is a quark or antiquark. The cross section is then proportional to the quark density inside the proton. The general expression for the differential cross section $ep \to e'H$ is

$$\frac{\mathrm{d}^2\sigma}{\mathrm{d}x\mathrm{d}Q^2} = \frac{4\pi\alpha^2}{xQ^4}\left[\left(1 - y + \frac{y^2}{2}\right) \cdot F_2(x, Q^2) - \frac{y^2}{2} \cdot F_L(x, Q^2)\right], \qquad (1)$$

where Z exchange has been neglected (it is a 1% correction for $Q^2 \approx 1000$ GeV^2). The structure function F_2 can be interpreted (in the "DIS" scheme) in terms of the quark and antiquark densities, q_i and $\bar{q}_i$, and their couplings to the photon, i.e. their charges e_{q_i}:

$$F_2(x, Q^2) = x \sum_i e_{q_i}^2 [q_i(x, Q^2) + \bar{q}_i(x, Q^2)], \tag{2}$$

where the sum runs over all quark flavours. The longitudinal structure function F_L vanishes in zero'th order α_s , and will be discussed later.

In the simple quark parton model the proton consists just of 3 valence quarks. Their distribution functions in fractional proton momentum x , $xq(x)$, would peak at $\approx 1/3$ and tend towards zero for $x \to 0, 1$. In a static model of the proton, they would not depend on Q^2 . It then follows that F_2 should not depend on Q^2 , just on x (Bjorken scaling).

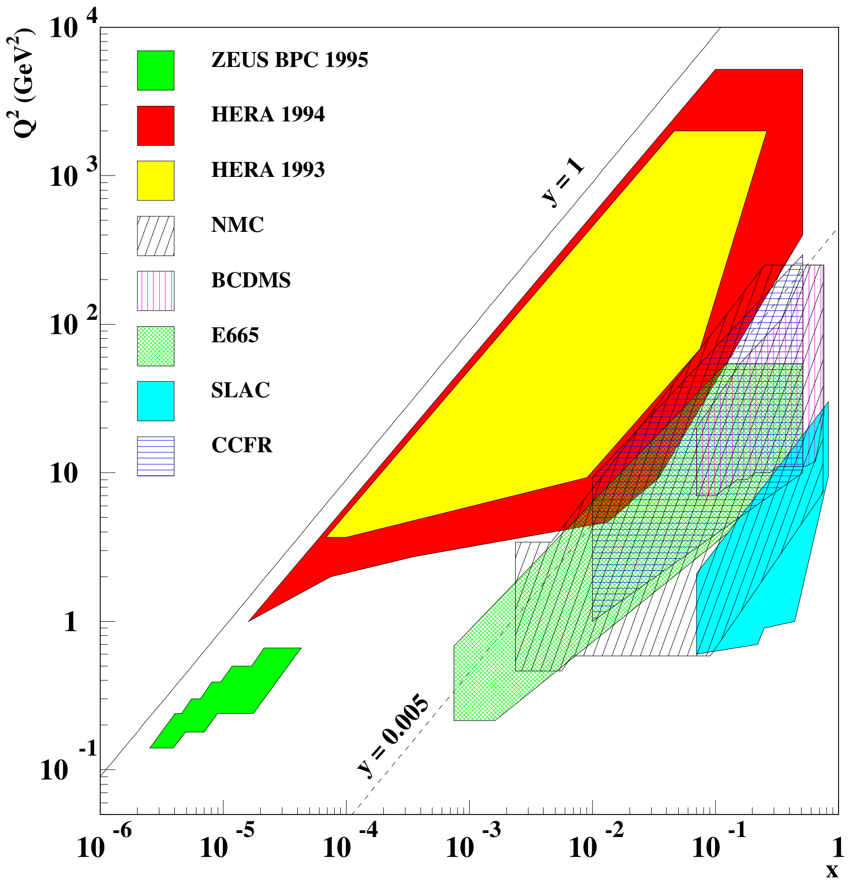

Figure 2: Coverage in the kinematic plane (x, Q^2) of various DIS experiments.

When QCD is "turned on" the quarks may radiate (and absorb) gluons, which in turn may split into quark–antiquark pairs or gluon pairs. More and more of these fluctuations can be resolved with increasingly shorter wavelength of the photonic probe, $\lambda = 1/Q$. With Q^2 increasing, we have a depletion of quarks at large x , and a corresponding accumulation at lower x. In addition, "sea quarks" from $g \to q\bar{q}$ splittings populate small x. In fact, at small x it is the gluon content with distribution function $g(x, Q^2)$ which governs the the proton and gives rise to the DIS cross section via $q\bar{q}$ pairs.

The dynamic features of DIS have been calculated in various approximations of QCD. One obtains equations for the Q^2 dependence of parton densities (and structure functions) like

$$\frac{\mathrm{d}q(x,Q^2)}{\mathrm{d}\ln Q^2} = \frac{\alpha_s(Q^2)}{2\pi} \int_x^1 \frac{dz}{z} \left[q(z,Q^2) P_{qq}(\frac{x}{z}) + g(z,Q^2) P_{qg}(\frac{x}{z}) \right], \tag{3}$$

(and similarly for the gluon densities), the famous DGLAP (Dokshitzer-Gribov-Lipatov-Altarelli-Parisi) equations [1]. They involve the calculable Altarelli-Parisi splitting functions $P_{ij}(z)$, which give the probability of parton branchings $q \to qg$, $g \to gg$ and $g \to q\bar{q}$, where the daughter parton i carries a fraction $1 - z$ of the mother's (j) momentum. The coupled integro-differential equations for the quark and gluon densities can be solved, allowing to calculate them for any value of Q^2, once they are known at a particular value Q_0^2.

For large Q^2 and for small x where the proton is dominated by gluons one obtains in the "double leading log" (DLL) approximation ($\ln\ln(Q^2/Q_0^2) \gg 1$, $\ln(1/x) \gg 1$) the formula [2]

$$xg(x,Q^2) \approx xg(x,Q_0^2) \exp\sqrt{\frac{144}{25} \ln \frac{\ln(Q^2/\Lambda^2)}{\ln(Q_0^2/\Lambda^2)} \ln(1/x)}. \tag{4}$$

At small x a fast rise of the gluon density is predicted. That is, xg increases faster than $(\ln \frac{1}{x})^\lambda$, but slower than $(\frac{1}{x})^\lambda$ for any power λ, the growth depending on the "evolution length" from Q_0^2 to Q^2.

2.1. The structure function F_2

ZEUS and H1 have measured F_2 in a completely new kinematic domain compared with fixed target experiments, most notably to much smaller values of x. The HERA data [3, 4] (Fig. 3) exhibit a steep rise of F_2 towards small x , which flattens at smaller Q^2. They signal increasing parton densities at smaller x.

In Fig.4 F_2 is shown as a function of Q^2 for fixed x values. At $x \approx 0.1$ scaling is observed – F_2 does not depend on Q^2 . At $x > 0.1$ F_2 decreases with Q^2 due to parton splittings, the products of which are found then at smaller x . Therefore F_2 increases with Q^2 for $x < 0.1$ in accord with the above qualitative discussion.

From a DGLAP evolution of pre-HERA data this sharp rise could not be predicted a priori, because input distributions at small x were not available. It was known though that asymptotically for $Q^2 \to \infty$ the small x behaviour is given by the DLL formula eq. 4. The interesting question is whether the HERA data are consistent with DGLAP evolution, or whether new effects have to be taken into account, which one may expect at very small x. The DGLAP evolution resums all leading terms $\sim (\alpha_s \ln(Q^2/Q_0^2))^n$, but neglects terms $\sim (\alpha_s \ln(1/x))^n$ in the perturbation series. The latter may become important at very small x ($\alpha_s \ln(1/x) \gg 1$) but moderate Q^2 , and are treated in the BFKL (Balitsky-Fadin-Kuraev-Lipatov) [5] equation. The BFKL equation predicts an even more dramatic growth (the "Lipatov growth") of the gluon density than the DLL expression at small x, $F_2 \sim xg(x) \sim x^{-\lambda}$, with $\lambda \approx 0.5$ in leading order (LO).

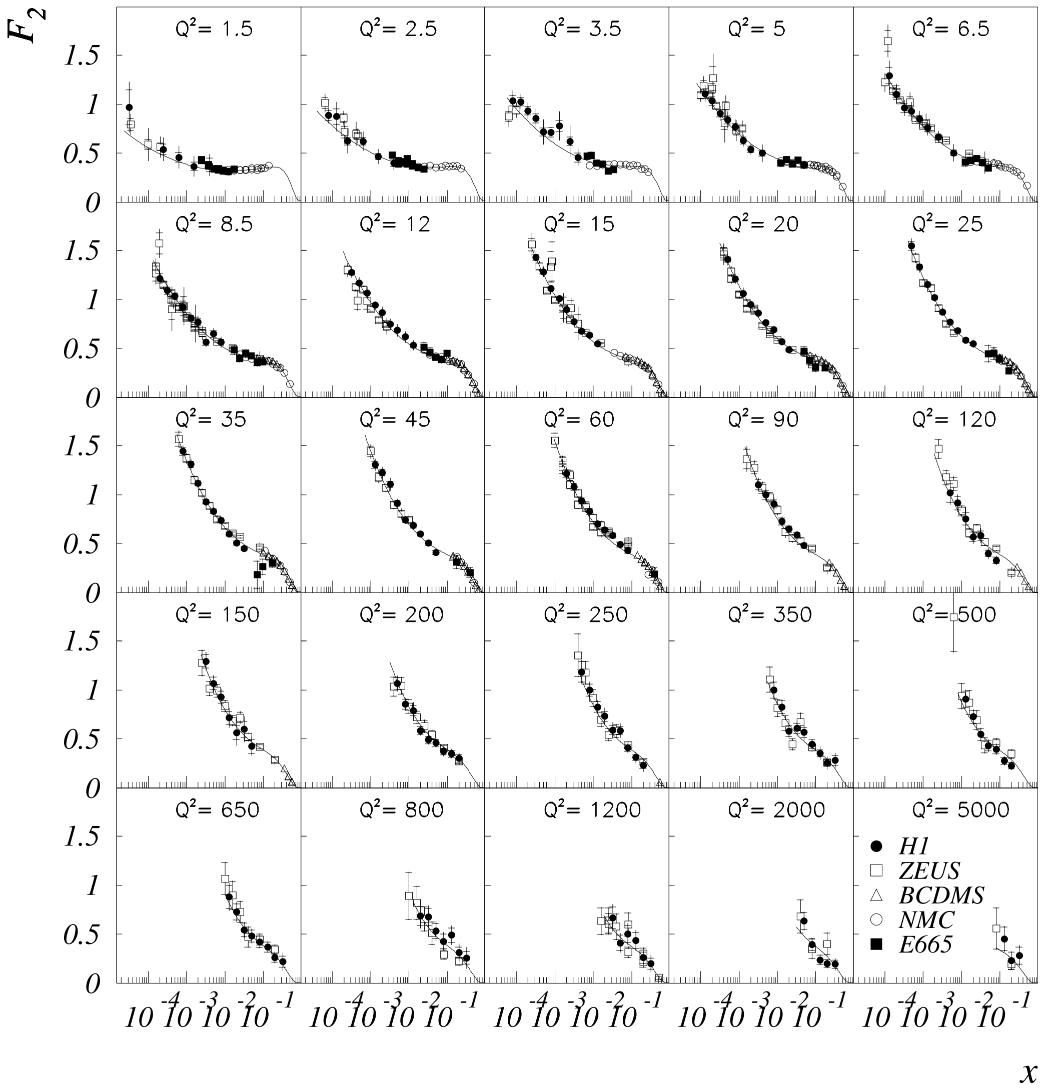

Figure 3: The structure functions $F_2(x, Q^2)$ as a function of x for different Q^2 bins. Shown are data from H1 [3], ZEUS [4], BCDMS [9], NMC [10] and E665 [11]. A NLO DGLAP QCD fit to the data with $Q^2 > 5GeV^2$ is shown as full line.

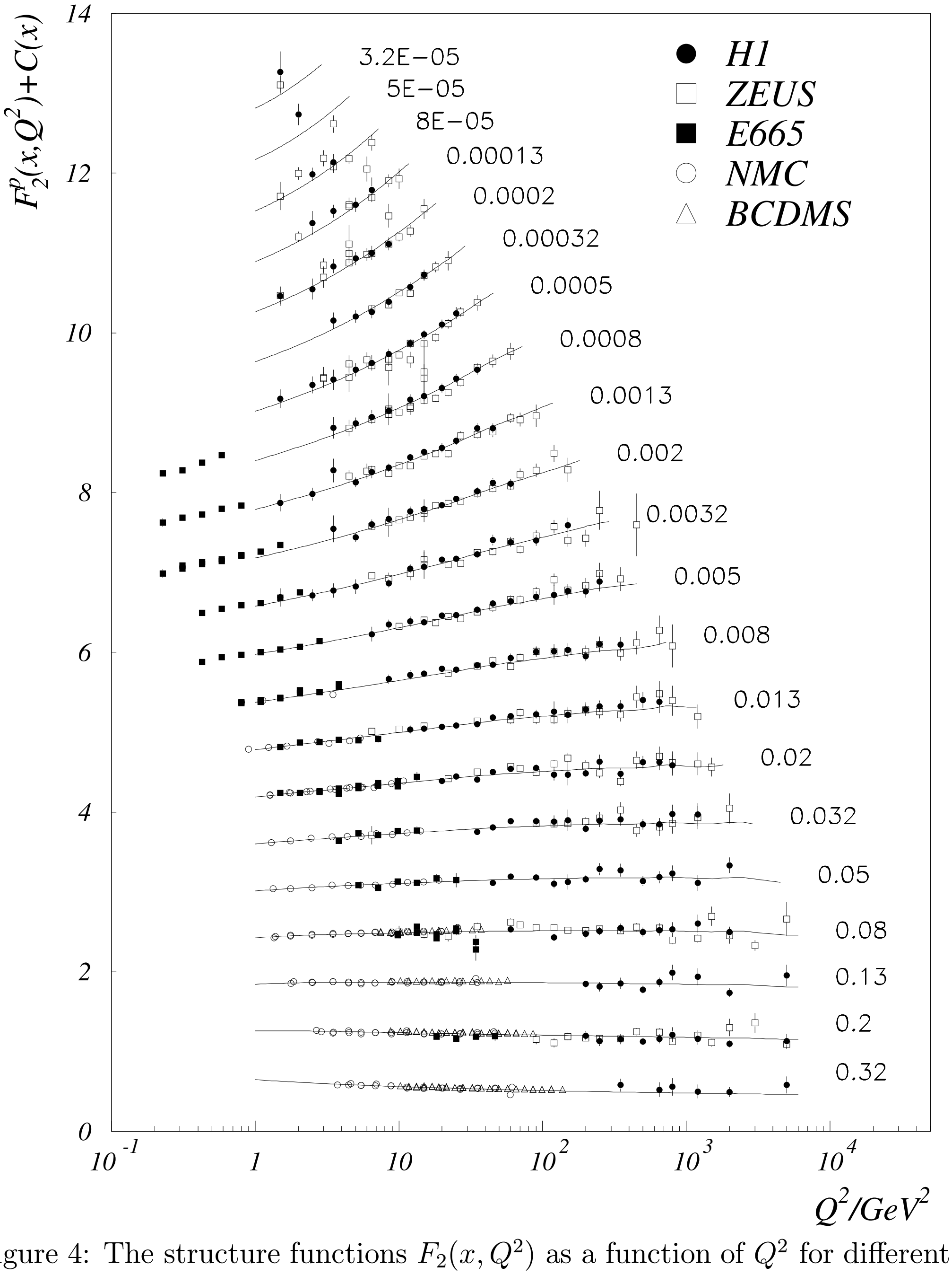

Figure 4: The structure functions $F_2(x,Q^2)$ as a function of Q^2 for different x bins. For better visibility, a function $C(x) = 0.6(i - 0.4)$, with i the x bin number ($i = 1$ for $x = 0.32$), is added to F_2 in the plot. Shown are the HERA and fixed target data, as well as a NLO QCD fit [3].

It turns out, however, that the data can be fit perfectly well with parton densities which obey the next-to-leading-order (NLO) DGLAP evolution equations (see Fig. 3) [4, 6]. Standard QCD evolution works over many orders of magnitude in both x and Q^2! H1 obtains values between 0.2 and 0.4 for the exponent in $F_2 \sim (1/x)^\lambda$, increasing with Q^2. In fact, both the x and the Q^2 dependence of F_2 can be attributed predominantly to the DLL formula, which can be displayed nicely with a suitable variable transformation ("double asymptotic scaling" [7]).

It is remarkable that the F_2 data can be described by evolving flat or valence-like input quark and gluon distributions from a very low scale, $Q_0^2 = 0.35$ GeV^2 up in Q^2 [8]. The steep rise with decreasing x is achieved by the long evolution length in Q^2 from the very low scale $Q_0^2 = 0.35$ GeV^2 (see eq. 4). The success of the GRV prediction came as a surprise for many, as perturbative QCD should only be applicable for Q^2 not too close to $\Lambda_{\text{QCD}} \approx 0.2$ GeV , because otherwise $\alpha_s\,(Q^2) = 12\pi/((33-2n_f)\ln(Q^2/\Lambda^2_{\text{QCD}}))$ diverges. It is quite satisfactory that the data can be described with parton densities following standard QCD evolution. However, the goal remains to calculate the measured magnitude of the growth $(1/x)^\lambda$ from QCD, rather than tuning it with the starting point Q_0^2 of the DLL evolution.

2.2. QCD analysis of F_2 – the gluon density and α_s

From the DGLAP eq. 3 it is clear that the scaling violations of F_2 depend on both α_s and the gluon density. In fact, for $x < 0.01$ and in lowest order one can derive the approximate formula [12]

$$\frac{\mathrm{d}F_2(x/2, Q^2\ )}{\mathrm{d}\ln Q^2} \approx \frac{10}{27}\frac{\alpha_s(Q^2)}{\pi} xg(x, Q^2), \tag{5}$$

because at small x the proton is dominated by gluons, and the scaling violations arise from quark pair creation from gluons. The full NLO QCD analysis now employed at HERA is of course more involved. Fig.5a shows the gluon density $x \cdot g(x, Q^2)$ extracted from the NLO QCD fit to the F_2 data. It increases sharply towards small x, the rise being more pronounced at larger Q^2.

Clearly, the density cannot increase forever; eventually saturation effects will have to be taken into account [13, 14]. When gluons of transverse size $\sim 1/Q$ fill up the whole transverse area offered by the proton, they will start to overlap and recombine. This would be a novel and very interesting situation indeed: high parton density, but Q^2 large enough for $\alpha_s\,(Q^2)$ to be small! Given the size of the proton $\approx$ 1fm, the critical condition for saturation effects to turn on can be estimated [14] as $x_{\text{crit}} g(x_{\text{crit}}, Q^2) \approx \frac{1\text{fm}^2}{1/Q^2} \approx 25\frac{Q^2}{\text{GeV}^2}$. This value is by far not reached by the measured gluon density (Fig.5a). It could be, however, that saturation does not set in uniformly over the proton's transverse area, but starts locally in so-called hot spots [15]. In this case x_{crit} would be larger. The data however do not require any saturation correction.

From an analysis of the scaling violations $\mathrm{d}F_2\ /\mathrm{d}\ln Q^2\ \sim \alpha_s$, or equivalently, of a QCD fit to the F_2 data, the strong coupling constant can be determined. From an analysis of the 1993 data $\alpha_s(m_Z\ ) = 0.120 \pm 0.005(\text{exp.}) \pm 0.009(\text{theor.})$ was obtained [16]. This is being updated for the higher statistics data now available [17].

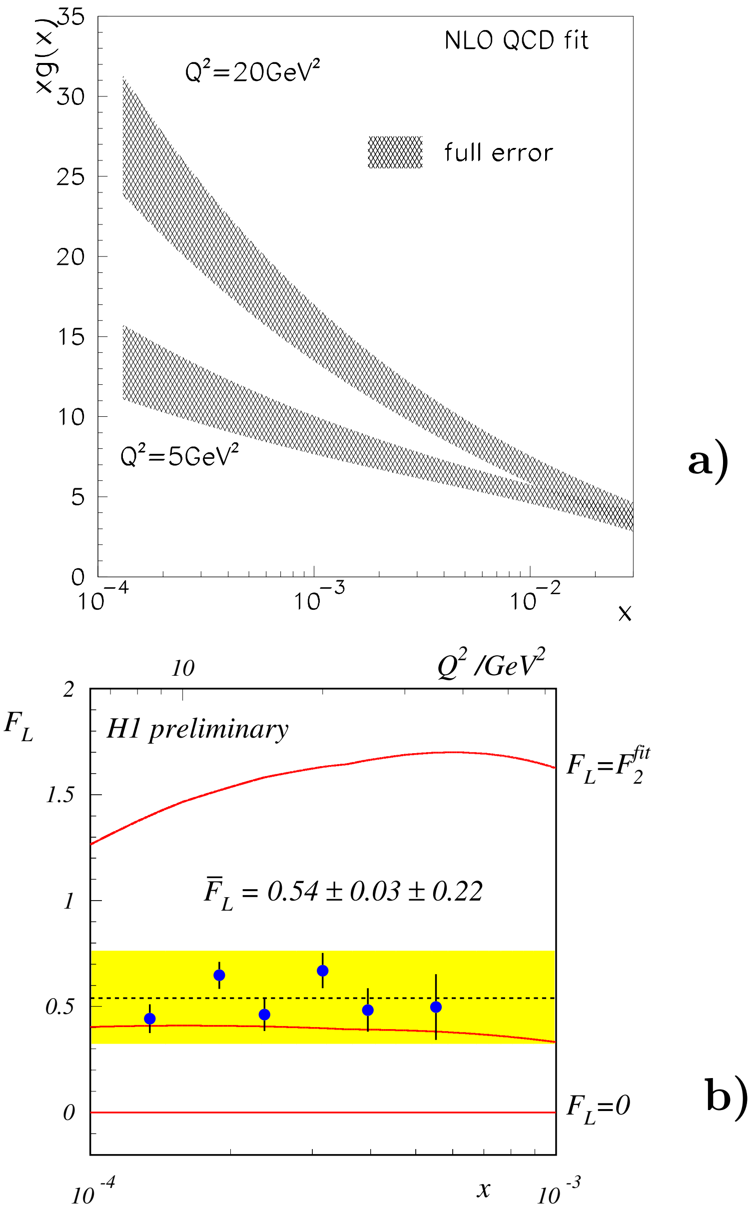

Figure 5: **a)** The gluon density $xg(x, Q^2)$ as extracted from a QCD analysis of the H1 F_2 data. **b)** The longitudinal structure functions F_L. The error bars represent statistical and systematic point-to-point errors. The error band gives an additional global systematic error. The QCD expectation based on the GRV [8] parton densities is also shown (solid line, unlabelled).

2.3. The longitudinal structure function F_L

The structure function F_2 can also be expressed in terms of the cross sections σ_T and σ_L for the absorption of transversely and longitudinally polarized virtual photons[2] on protons: $\sigma_{\rm tot}^{\gamma^* p} = \sigma_L + \sigma_T$, namely

$$F_2 = \frac{Q^2(1-x)}{4\pi^2\alpha}\frac{Q^2}{Q^2+4m_p^2x^2}\cdot\sigma_{\rm tot}^{\gamma^* p} \approx \frac{Q^2}{4\pi^2\alpha}(\sigma_L + \sigma_T), \qquad (6)$$

where the small x approximation has been applied. Similarly,

$$F_L = \frac{Q^2(1-x)}{4\pi^2\alpha}\cdot\sigma_L \approx \frac{Q^2}{4\pi^2\alpha}\cdot\sigma_L . \qquad (7)$$

Longitudinal photons have helicity 0 and can exist only virtually. In the QPM, helicity conservation at the electromagnetic vertex yields the Callan-Gross relation, $F_L = 0$, for scattering on quarks with spin 1/2. This does not hold when the quarks acquire transverse momenta from QCD radiation. Instead, QCD yields [19]

$$F_L(x,Q^2) = \frac{\alpha_s}{4\pi}x^2\int_x^1\frac{dz}{z^3}\left[\frac{16}{3}F_2(z,Q^2) + 8\sum_i e_{q_i}^2(1-\frac{x}{z})\cdot g(z,Q^2)\right], \qquad (8)$$

exposing the dependence of F_L on the strong coupling and the gluon density, which dominates over the first term at small x. In fact $F_L(x,Q^2) = 0.7\cdot[4\alpha_s/(3\pi)]\cdot xg(2.5x,Q^2)$ is not a bad approximation for $x < 10^{-3}$ [20].

The extraction of F_2 from the cross section measurement (eq. 1) so far had to make an assumption for F_L, because there existed no data in the HERA regime. At large y, $y \approx 0.7$, this is a 10% correction. The argument can be turned around, and F_L can be extracted at large y from a measurement of the cross section, assuming that F_2 follows a QCD evolution and can be extrapolated from measurements at smaller y. This procedure has been performed by H1 [21] (Fig.5b). The result $F_L = 0.54 \pm 0.03 \pm 0.22$ excludes the extreme possibilities $F_L = F_2$ and $F_L = 0$ and im plies $R \equiv \sigma_L/\sigma_T = F_L/(F_2 - F_L) \approx 0.5$, since $F_2 \approx 1.5$. This is self consistent with the gluon density extracted from the H1 QCD fit.

2.4. The very low Q^2 region

The ZEUS collaboration had for the 1994 run a new beam pipe calorimeter installed to cover small electron scattering angles. They can now access Q^2 values below 1 GeV^2 which had previously been the realm of fixed target experiments, see Fig.6 [22]. Will perturbative QCD still hold at such a low scale? The perturbatively evolved parton densities of GRV can describe the data down to $Q^2 \approx 1.5$ GeV^2 . Below $Q^2 \approx 0.4$ GeV^2 the GRV curves turn over and become valence like, by far failing to account for the data. A nonperturbative model by Donnachie-Landshoff [23],

[2] We use the Hand convention [18] for the definition of the virtual photon flux.

which is based on Regge phenomenology and reproduces the total photoproduction cross section ($Q^2 \approx 0$) gives a good description of the data in this regime, but fails above $Q^2 \ \approx 2$ GeV^2 . The transition from perturbative to non-perturbative QCD appears to be rather fast.

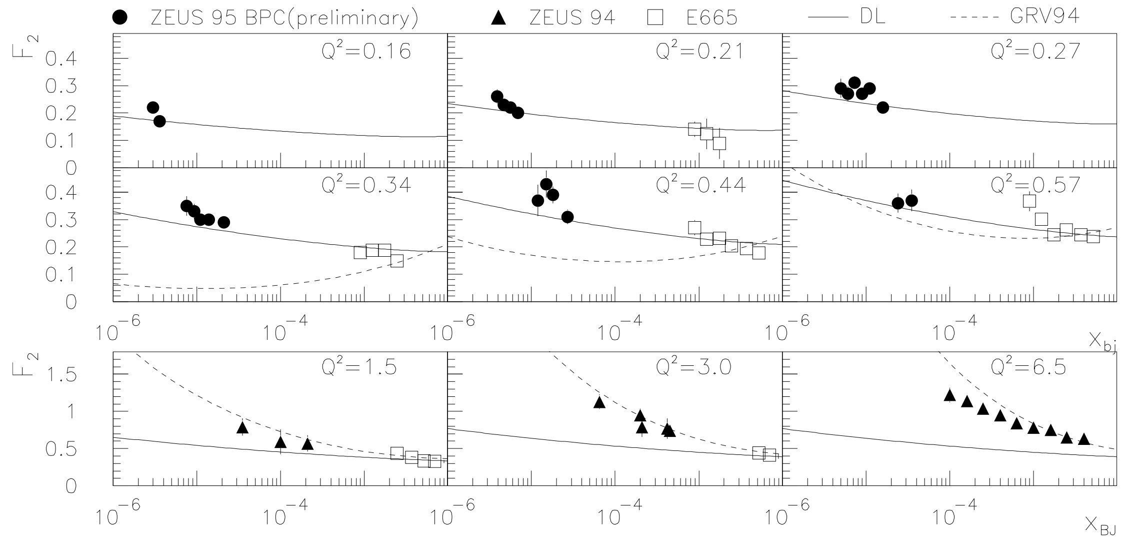

Figure 6: The structure function F_2 measured at small Q^2 by ZEUS [22]. Overlayed are the expectations from the Donnachie-Landshoff [23] Regge model (DL), and from the perturbatively evolved parton densities from Glück, Reya, Vogt [8] (GRV).

3. The hadronic final state

New insights into both perturbative QCD and confinement can be gained by studying the hadronic final state, thereby providing complementary information to the totally inclusive structure function measurements. For example, footprints of BFKL dynamics are being searched for in especially devised observables (E_T flows, forward jets, high p̂articles). F_2 may be too inclusive to be sensitive to these effects, because all possible paths in the parton evolution are integrated over. Differences between DGLAP and BFKL evolution can be expected for the hadronic final state, because in DGLAP the phase space for parton radiation, basically given by W, is restricted by strong ordering of the transverse momenta k_T of subsequently emitted partons, which is not the case for BFKL (Fig.7a).

There exists also a possibility to discover new QCD effects, for example spectacular QCD instanton events. At a more "down to earth" level, the large phase space for hard QCD radiation (W up to 300 GeV) can be exploited for the extraction of the strong coupling constant from jet rates and other final state obervables. For both cases, the searches for new effects and precision measurements, a good understanding of the final state dynamics in parton showers and hadronization is a prerequisite for meaningful results.

a)

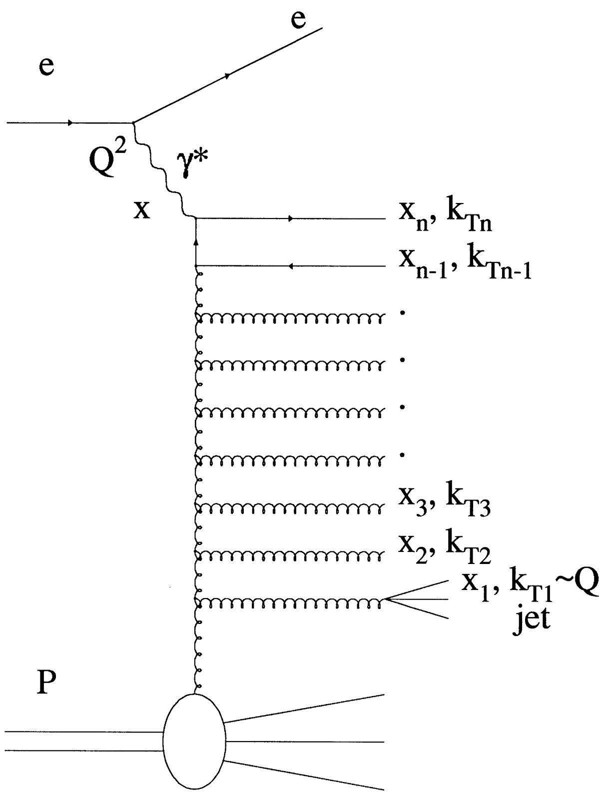

b)

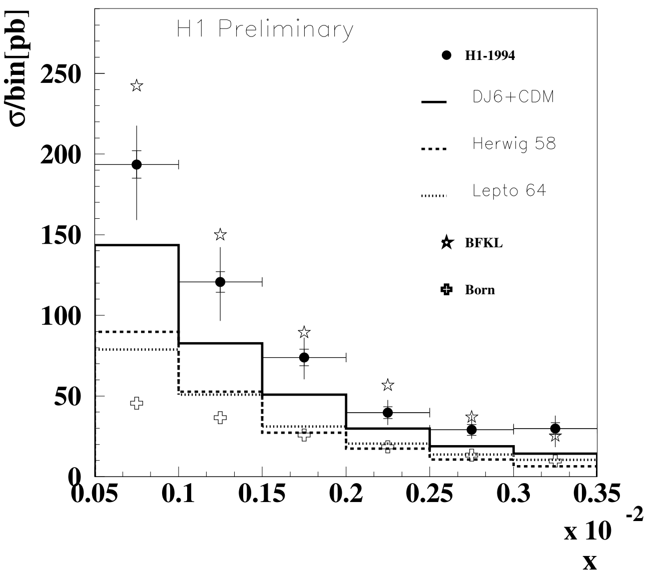

Figure 7: **a)** A ladder graph for parton evolution. The selection of forward jets in DIS events is illustrated. **b)** The cross section for forward jets as a function of x. Overlayed are QCD model predictions for hadron jets, and BFKL and Born graph calculations for partons. The jets are selected with $x_{\mathrm{jet}} > 0.035$, $0.5 < {k_{T\mathrm{jet}}}^2/Q^2 < 2$ and $k_{T\mathrm{jet}} > 3.5$ GeV .

Apart from the laboratory frame, the hadronic centre of mass system (CMS) and the Breit frame are used in the analyses. The Breit frame is defined by the condition that the virtual photon does not transfer energy, only momentum. In the QPM picture the scattering quark would thus just reverse the direction of its momentum of magnitude $Q/2$. The CMS is defined as the centre of mass system of the incoming proton and the virtual boson, i.e. the CMS of the hadronic final state with invariant mass W. In both systems the hemisphere defined by the virtual photon direction is referred to as the current region, the other (containing the proton remnant) as the target region. The CMS current and target systems are back to back with momentum $W/2$ each. Longitudinal and transverse quantities are calculated with respect to the boson direction.

3.1. QCD models

The complexity of the hadronic final state makes analytical QCD calculations often very difficult—there exist but a few. Indispensable tools for the study of the hadronic final state are therefore Monte Carlo models which simulate the underlying dynamics. They incorporate QCD evolution and parton radiation in different approximations and utilize phenomenological models for the non-perturbative hadronization phase. The MEPS model (Matrix Element plus Parton Shower), an option of the LEPTO generator [24], incorporates the QCD matrix elements up to first order, with additional soft emissions generated by adding leading log parton showers. In the colour dipole model (CDM, generator ARIADNE) [25, 26] radiation stems from a chain of independently radiating dipoles formed by the colour charges. The HERWIG model [27] is also based on leading log parton showers, with additional matrix element corrections [28]. The CDM description of gluon emission is similar to that of BFKL evolution to the extent that the gluons emitted by the dipoles do not obey strong ordering in k_T [29]. In the MEPS and HERWIG models the partons emitted in the cascade are strongly ordered in k_T, because they are based on leading log DGLAP parton showers.

3.2. Transverse energy flow

It can be shown [30] that DGLAP evolution corresponds to the evaluation of ladder graphs (Fig.7) in which subsequently emitted gluons are strongly ordered in transverse momenta k_T , $Q_0^2 \ll k_T{}_1^2 \ll ...k_T{}_j^2 \ll ...Q^2$. In the BFKL evolution on the other hand gluon emission is not restricted by strong ordering, the emitted gluons rather follow a kind of random walk in k_T space. As a consequence, one expects more gluon radiation and hence more transverse energy E_T emitted in the rapidity region between the remnant and the current systems [31]. The HERA data [32, 33] are compatible with the predicted magnitude [31] and the characteristic increase towards small x from the BFKL calculation (Fig.8). However, measured are hadrons, but the calculations do not include hadronization! It turns out that

DGLAP models with large hadronization corrections to the partonic E_T are also able to describe the data [34, 35], precluding strong conclusions on BFKL dynamics from the E_T data.

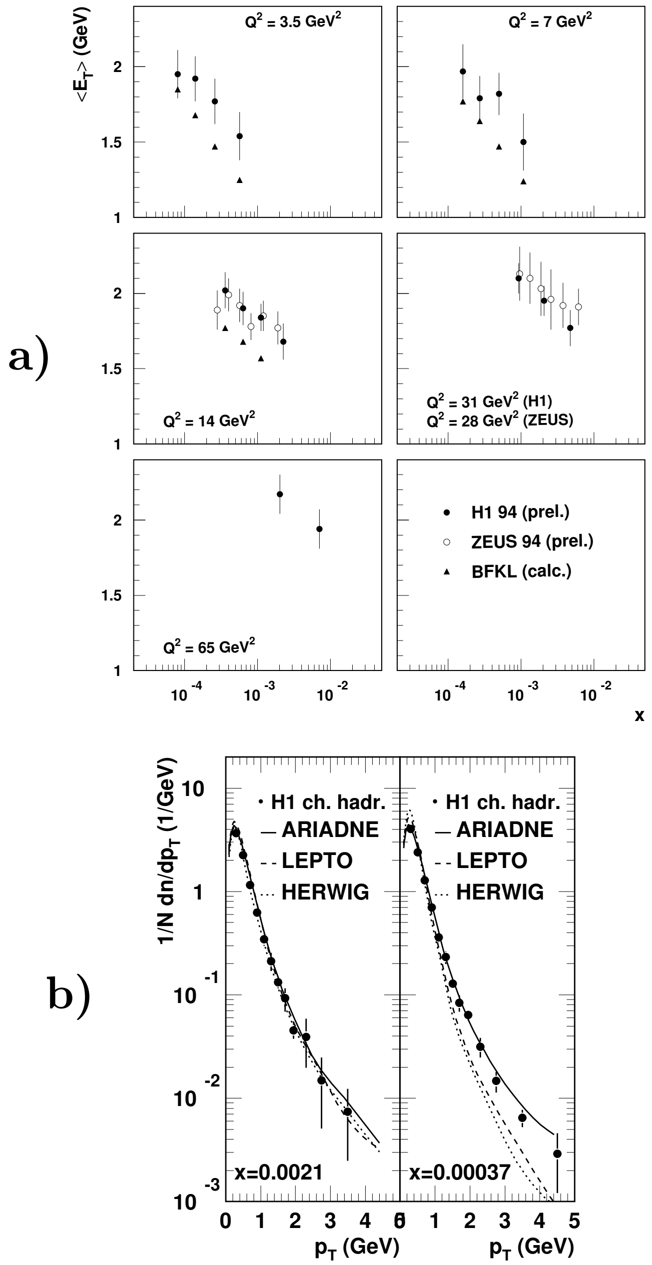

Figure 8: **a)** The average hadronic E_T vs. x, measured in $-0.5 < \eta < 0.5$ in the CMS from H1 [32] and ZEUS [33] (both preliminary). The BFKL calculation [31] at the parton level is also shown. **b)** The charged particle spectra measured in $0.5 < \eta < 1.5$ in the CMS by H1 for high and for low x at $Q^2 \approx 14$ GeV , and the predictions from the colour dipole model (ARIADNE), LEPTO and HERWIG. The plots are normalized to the total number of events N.

3.3. Inclusive transverse momentum spectra

Another method to probe the low x parton dynamics is to look for high particles [36]. They signal the presence of hard gluons, while hadronization can only produce limited. Perturbative parton radiation can thus be disentangled from hadronization effects, which pose a problem for the interpretation of the E_T data. H1 finds at low x and at central rapidity significantly harder spectra than expected from Monte Carlo calculations based upon LO matrix element and leading log DGLAP parton showers (Fig.8b). The colour dipole model, in which parton radiation is more abundant, gives a good description of the data. QCD calculations and BFKL Monte Carlo predictions for these spectra are eagerly awaited to find out whether the enhanced parton radiation can indeed be attributed to BFKL evolution, or to something else, perhaps even more interesting.

3.4. Forward jets

A classic signature for BFKL dynamics [37, 38] is the production of "forward jets" with $x_{\rm jet} = E_{\rm jet}/E_p$, the ratio of jet energy and proton beam energy, as large as possible, and with transverse momentum $k_{T{\rm jet}}$ close to Q in order to reduce the phase space for the k_T ordered DGLAP evolution (see Fig.7). An enhanced rate of events with such jets is thus expected in the BFKL scheme [37]. The experimental difficulty is to detect these "forward" jets which are close to the beam hole in the proton direction. The rate of forward jets measured by H1 [39] (Fig.7b) increases with falling x. This is expected from BFKL calculations, in contrast to calculations without the BFKL ladder [40]. The behaviour of the data is better represented by the CDM than by the DGLAP representative, the MEPS model. However, the cross sections are calculated [40] for partons, while experiments measure hadron jets. This gap has to be bridged from both sides to allow a strictly valid comparison.

3.5. Instantons

The standard model contains processes which cannot be described by perturbation theory, and which violate classical conservation laws like baryon and lepton number in the case of the electroweak sector and chirality for the strong interaction [41]. Such anomalous processes are induced by instantons [42]. At HERA, QCD instantons may lead to observable effects in the hadronic final state in DIS [43, 44]. The instanton should decay isotropically into a high multiplicity state, consisting of gluons and all quark flavours (in each event!) which are kinematically allowed. Due to the isotropic decay, one expects a densely populated region in rapidity, other than the current jet, which is isotropic in azimuth. The presence of strangeness and charm provides an additional signature (Fig.9a). H1 does not see an excess of K^0 production over the prediction from standard QCD models (Fig.9) [45]. At most a few percent admixture of instanton events is allowed to normal DIS, corresponding to an upper limit for the instanton cross section for $x > 0.001$ of 0.95 nb. In the future, more elaborate search strategies and larger luminosities offer the chance for a fundamental discovery at HERA [46]!

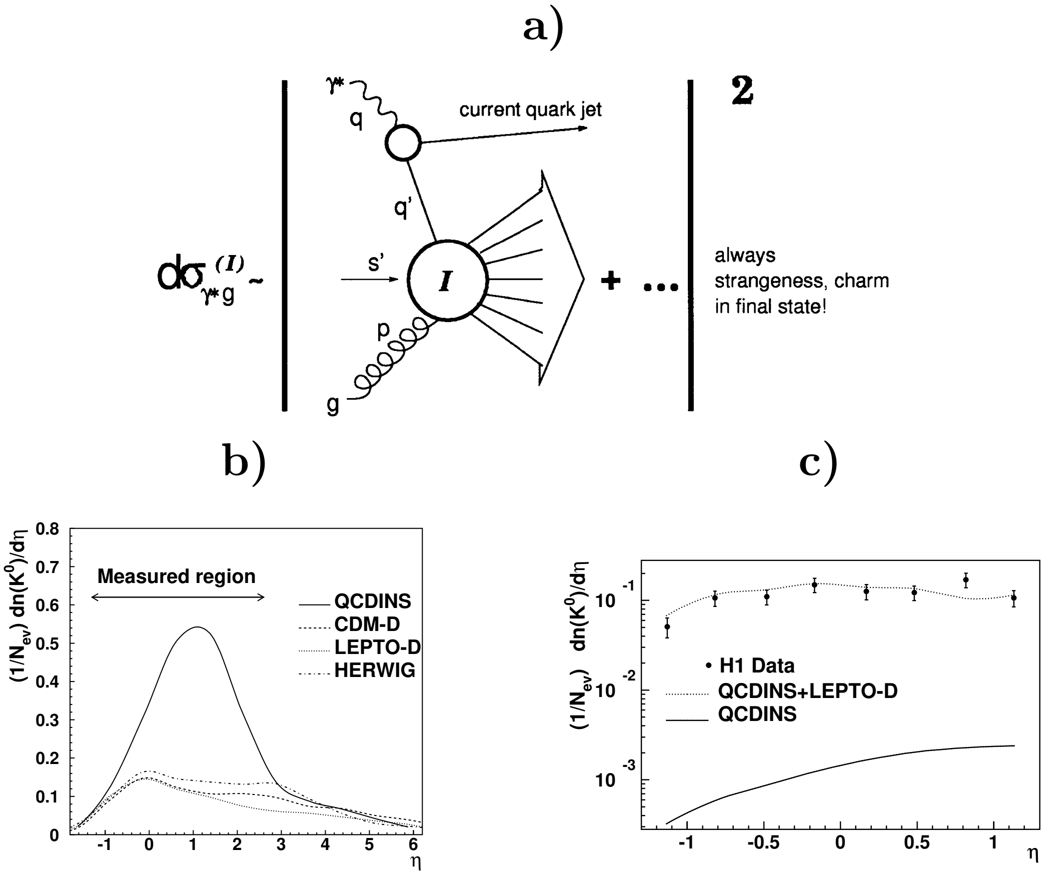

Figure 9: **a)** Instanton induced process, and the K^0 yield as a function of laboratory pseudorapidity η. The proton direction is to the right. Shown in **b)** are the predictions from standard QCD models, and from an instanton model (QCDINS). In **c)** the H1 data [45] are overlayed with the prediction of a standard QCD model plus a 0.6% instanton contribution, and with the maximally allowed fraction of instanton events (QCDINS).

3.6. The running coupling constant α_s from jet rates

The processes contributing to jet production in DIS up to first order in α_s are shown in Figs.1, 10. The QPM process results in a so-called "1+1" jet topology, while the QCDC and BGF processes give "2+1" jet events, where the "+1" refers to the unobserved remnant jet. Since the rate of 2+1 jet production is $\propto \alpha_s$, $\alpha_s(Q)$ can be measured [47, 48], and the scale dependence can be studied. The ZEUS data of 1994 are shown in Fig.10. The Q dependence is as expected for a running α_s . A fit yields $\alpha_s(m_Z) = 0.117 \pm 0.005(\text{stat.})^{+0.004}_{-0.005}(\text{syst.}) \pm 0.007(\text{theor.})$, to be compared with the world average, $\alpha_s(m_Z) = 0.117 \pm 0.005$. It can be expected that the theoretical uncertainties can be reduced by studying different jet algorithms [49], and by obtaining a better understanding of the hadronic final state dynamics.

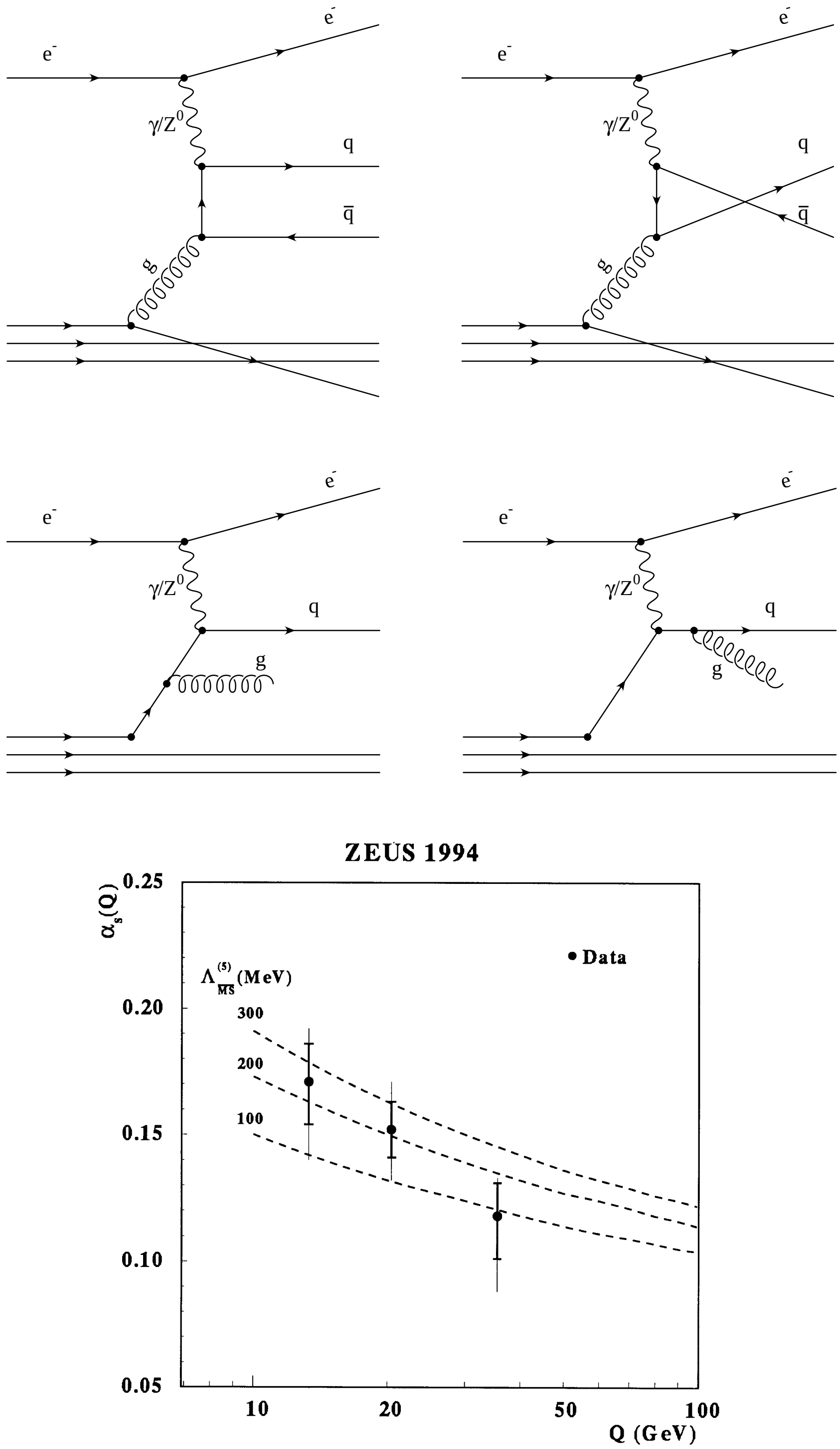

Figure 10: Determination of the strong coupling constant. Shown are the boson-gluon fusion (BGF) and the QCD Compton (QCDC) graphs, giving rise to 2+1 jet events, and the measured α_s as a function of Q from the ZEUS jet rates[48].

3.7. Thrust in the Breit frame

In the Breit frame in- and outgoing quark have equal but opposite sign momenta $Q/2$ (QPM picture), and in e^+e^-annihilation the outgoing quark and antiquark have equal but opposite momenta $\sqrt{s}/2 = Q/2$. Due to this similarity it is interesting to compare measurements in the Breit current hemisphere in DIS with e^+e^-data. The current hemisphere of the DIS Breit frame is equivalent to one hemisphere of the $e^+e^- \to q\bar{q}$ reaction. DIS experiments have the advantage that they cover a large span in Q^2 in a single experiment.

Infrared safe event shape variables have in the past been a very useful way to measure α_s , because it was possible to calculate them in QCD. One example is the thrust T, where T is the normalized sum of all longitudinal particle momenta with respect to the thrust axis n_T:

$$T = \max \frac{\sum |\vec{p_i} \cdot \vec{n}_T|}{\sum |\vec{p_i}|}. \tag{9}$$

$\vec{n}_T$ is varied to maximize the thrust. $T = 1$ when all particles are collinear, and $T = 0.5$ for an isotropic distribution. The measured thrust value in the Breit current hemisphere [50] increases with increasing Q (i.e. increasing energy of the scattered quark) – the current jet becomes more collimated (Fig.11). The data agree well with what has been measured in e^+e^-experiments. The advantage at HERA is evident: the evolution with Q can be studied in a single experiment. In fact the data can be fit with a QCD ansatz $\langle 1 - T \rangle = c_1 \cdot \alpha_s\ (Q) + c_2 \cdot \alpha_s\ ^2(Q) + c_3 \cdot 1/Q$, where the first terms are perturbative up to NLO, and the last term parametrizes all higher orders and non-perturbative hadronization effects with a power correction [51]. The HERA data will allow to check the hypothesized universality of the power correction, and to extract $\alpha_s(Q)$ once the NLO coefficient has been calculated.

3.8. Scaling violations of charged particle spectra

The transition from partons to hadrons can be described with fragmentation functions $D(z, Q)$, which give the probability to find a hadron carrying the momentum fraction z of the original parton's momentum. These functions are universal, and exhibit scaling in lowest order, i.e. they are independent of Q. In DIS one can measure the momentum spectra in the scaled variable $x_p = p/(Q/2))$, where p is the hadron momentum and $Q/2$ the maximal possible momentum in the Breit frame. When QCD radiation is switched on, the original quark may radiate a gluon, and instead of one hard parton to fragment there are now two softer ones, which result in a softer x_p spectrum. These scaling violations increase with Q, as the phase space for QCD radiation increases. The preliminary ZEUS data [52] on x_p (Fig.11) indeed show that with increasing Q there are less hadrons with large x_p, and more hadrons with small x_p. These scaling violations are analogous to the scaling violations of F_2 , and can be used in a similar fashion to extract α_s [53].

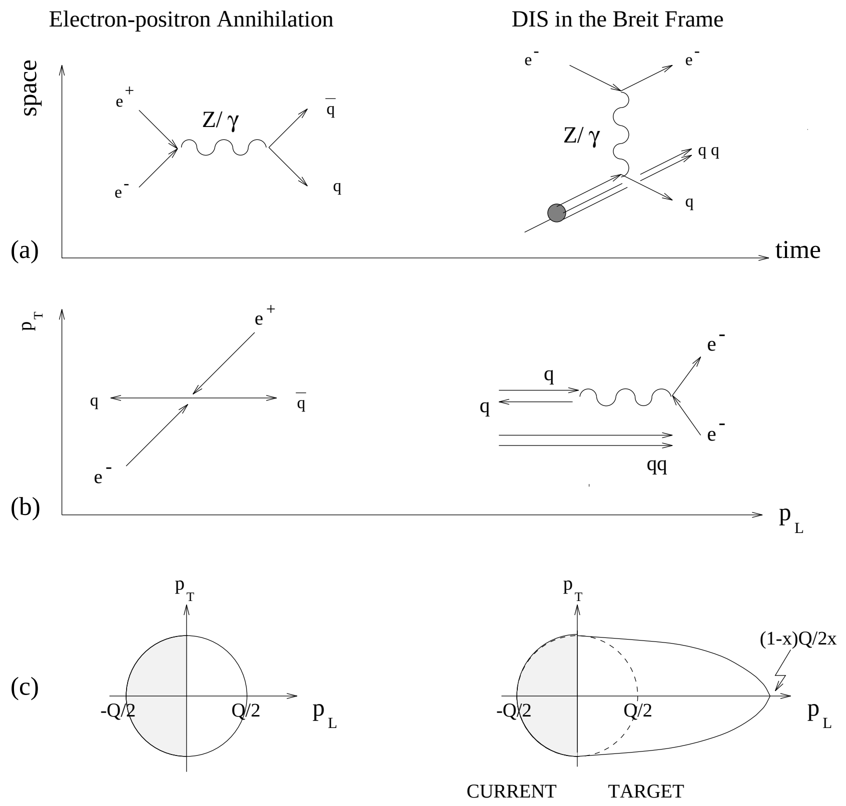

Electron-positron Annihilation
DIS in the Breit Frame
space
time
Z/ γ
(a)
(b)
(c)
p
T
p
L
-Q/2
Q/2
(1-x)Q/2x
CURRENT
TARGET

a)

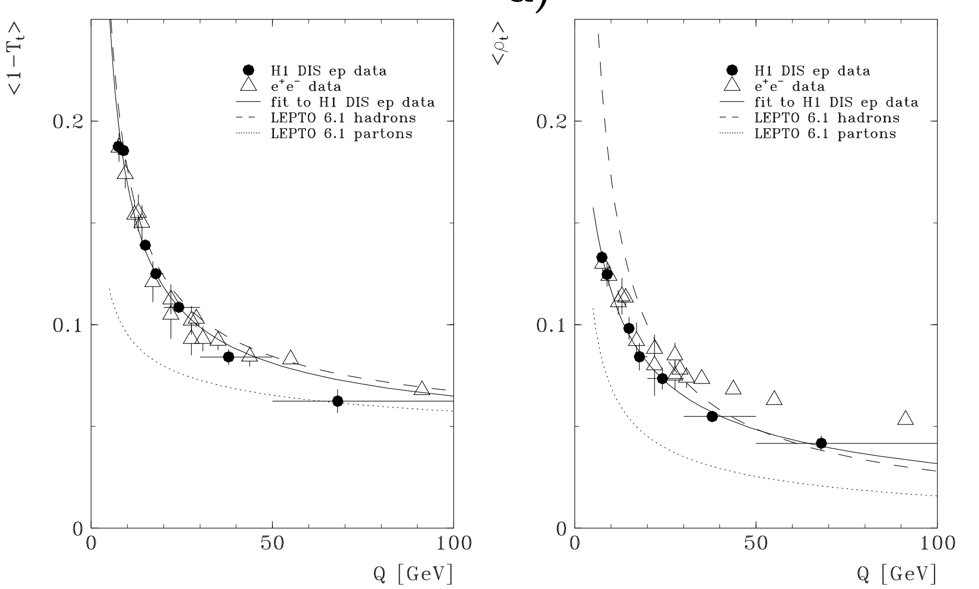

<1−T_t>
<ρ_t>
H1 DIS ep data
e+e− data
fit to H1 DIS ep data
LEPTO 6.1 hadrons
LEPTO 6.1 partons
Q [GeV]

b)

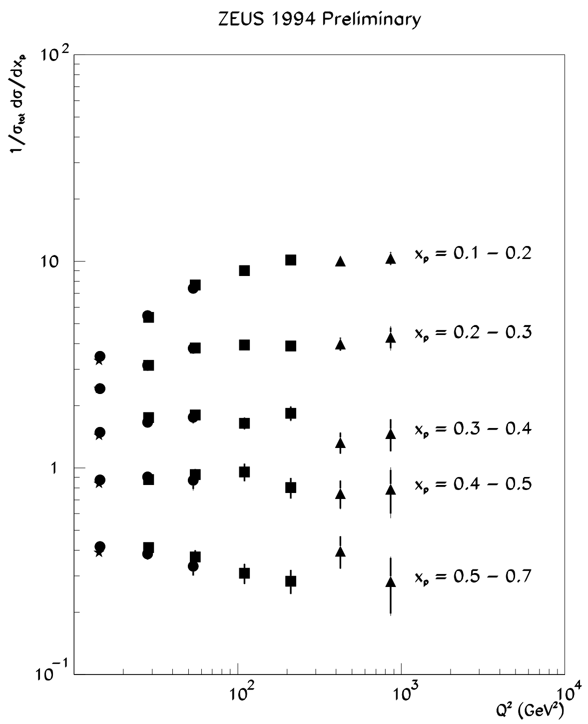

Figure 11: QCD analysis in the Breit frame (see sketch). **a)** The average $1-T$ (T=thrust) measured in the Breit frame as a function of Q. The data are compared to e^+e^-data and to the LEPTO program, both for hadrons and for partons. A QCD fit to the data is also shown. **b)** The normalized charged particle cross section in bins of $x_p = 2p/Q$ as a function of Q^2 [52].

4. Conclusions

HERA has already delivered a wealth of information about the structure of the proton, in particular about partons which carry a small fraction of the proton's momentum. Standard QCD evolution gives a good description of the inclusive structure function measurements. Novel QCD effects are being searched for in the hadronic final state with some interesting signals emerging, the interpretation of which is under discussion. In addition, the strong coupling constant is being determined using a variety of hadronic final state observables. These analysis profit from the fact that the scale at which the coupling constant is being determined can be varied in a single experiment at HERA.

5. Acknowledgements

It is a pleasure to thank A.A. Logunov for the kind invitation to this workshop, and A.V. Kisselev and V.A. Petrov for their hospitality during the conference. I would also like to thank my colleagues from H1 and ZEUS for providing me with the latest data, and J. Dainton, R. Eichler and R. Klanner for their careful reading of the manuscript.

References

[1] Yu. L. Dokshitzer, Sov. Phys. JETP 46 (1977) 641;
V.N. Gribov and L.N. Lipatov, Sov. J. Nucl. Phys. 15 (1972) 438 and 675;
G. Altarelli and G. Parisi, Nucl. Phys. 126 (1977) 297 .

[2] A. DeRujula et al., Phys. Rev. D10 (1974) 1649
B. Badelek et al., J. Phys. G.: Nucl. Part. Phys. 22 (1996) 815.

[3] H1 Collab., T. Ahmed et al., Nucl. Phys. B439 (1995) 471.

[4] ZEUS Collab., M. Derrick et al., Z. Phys. C69 (1996) 607; DESY 96-076.

[5] E.A. Kuraev, L.N. Lipatov and V.S. Fadin, Sov. Phys. JETP 45 (1972) 199;
Y.Y. Balitsky and L.N. Lipatov, Sov. J. Nucl. Phys. 28 (1978) 282.

[6] H1 Collab., S. Aid et al., Nucl.Phys. B470 (1996) 3.

[7] R.D. Ball and S. Forte, Phys. Lett. B335 (1994) 77, ibid. B336 (1994) 77.

[8] M. Glück, E. Reya, A. Vogt, Z. Phys. C67 (1995) 433.

[9] BCDMS Collab., A.C. Benvenuti et al., Phys. Lett. B223 (1989) 485; CERN-EP/89-06.

[10] NMC Collab., M. Arneodo et al., Phys. Lett. B364 (1995) 107.

[11] E665 Collab., M.R. Adams et al., FNAL-PUB-95/396-E.

[12] K. Prytz, Phys. Lett. B311 (1993) 286.

[13] J. Bartels and J. Feltesse, Proc. of the Workshop on Physics at HERA, Hamburg 1991, eds. W. Buchmüller and G. Ingelman, vol. 1, p. 131;
E.M. Levin, Proc. QCD – 20 Years Later, Aachen 1992, eds. P.M. Zerwas, H.A. Kastrup, vol. 1, p. 310 .

[14] A.H. Mueller, J. Phys. G, Nucl. Par. Phys. 19 (1993) 1463.

[15] A.H. Mueller and H. Navelet, Nucl. Phys. B282 (1987) 727.

[16] R.D. Ball and S. Forte, Phys. Lett. B358 (1995) 365.

[17] R.D. Ball and S. Forte, hep-ph/9607289;
A. DeRoeck, M. Klein and Th. Naumann, Phys. Lett. B385 (1996) 411.

[18] L.N. Hand, Phys. Rev. 129 (1963) 1834.

[19] A. Zee, F. Wilczek and S.B. Treiman, Phys. Rev. D10 (1974) 2881;
G. Altarelli and G. Martinelli, Phys. Lett. B76 (1978) 89.

[20] A.M. Cooper-Sarkar et al. , Z. Phys. C39 (1988) 281;
A.M. Cooper-Sarkar, R.C.E. Devenish and M. Lancaster, Proc. of the Workshop on Physics at HERA, Hamburg 1991, eds. W. Buchmüller and G. Ingelman, vol. 1, p. 155.

[21] H1 Collab., contrib. paper pa02-069 to ICHEP96, Warsaw 1996.

[22] ZEUS Collab., contrib. paper pa02-025 to ICHEP96, Warsaw 1996.

[23] A. Donnachie and P.V. Landshoff, Z. Phys. C61 (1994) 139.

[24] G. Ingelman, Proc. of the Workshop on Physics at HERA, Hamburg 1991, eds. W. Buchmüller and G. Ingelman, vol. 3, p. 1366 .

[25] G. Gustafson, Ulf Petterson, Nucl. Phys. B306 (1988);
G. Gustafson, Phys. Lett. B175 (1986) 453;
B. Andersson, G. Gustafson, L. Lönnblad, Ulf Petterson, Z. Phys. C43 (1989) 625 .

[26] L. Lönnblad, Comp. Phys. Comm. 71 (1992) 15.

[27] G. Marchesini et al.,Comp. Phys. Comm. 67 (1992) 465 .

[28] M. Seymour, Lund preprint LU-TP-94-12 (1994); Nucl. Phys. B436 (1995) 443.

[29] L. Lönnblad, Z. Phys. C65 (1995) 285; CERN-TH/95-95;
A. H. Mueller, Nucl. Phys. B415 (1994) 373 .

[30] Yu. L. Dokshitzer, Sov. Phys. JETP 46 (1977);
A. Martin, Durham preprint DTP/93/66 .

[31] J. Kwieciński, A.D. Martin, P.J. Sutton and K.Golec-Biernat, Phys. Rev. D50 (1994) 217;
K.Golec-Biernat, J. Kwieciński, A.D. Martin and P.J. Sutton, Phys. Lett. B335 (1994) 220.

[32] H1 Collab., contrib. paper pa02-073 to ICHEP'96, Warsaw 1996.

[33] N. Pavel, Proc. of the DIS96 workshop, Rome 1996.

[34] A. Edin, G. Ingelman and J. Rathsman, Phys.Lett. B366 (1996) 371;DESY 96-060.

[35] T. Carli, Proc. of the DIS96 Workshop, Rome 1996.

[36] M. Kuhlen, Phys. Lett. B382 (1996) 441.

[37] A.H. Mueller, Nucl. Phys. B (Proc. Suppl.) 18C (1990) 125; J. Phys. G17 (1991) 1443.

[38] J. Bartels, A. De Roeck, M. Loewe, Z. Phys. C54 (1992) 635;
W.K. Tang, Phys. Lett. B278 (1992) 363.

[39] H1 Collab., contrib. paper pa03-049 to ICHEP'96, Warsaw 1996.

[40] J. Kwieciński, A.D. Martin, P.J. Sutton, Phys. Rev. D46 (1992) 921;
J. Bartels et al., DESY-96-036.

[41] G. 't Hooft, Phys. Rev. Lett. 37 (1976) 8; Phys. Rev. D14 (1976) 3432.

[42] A. Belavin, A. Polyakov, A. Schwarz and Yu. Tyupkin, Phys. Lett. B59 (1975) 85.

[43] A. Ringwald, Nucl. Phys. B330 (1990) 1;
O. Espinosa, Nucl. Phys. B343 (1990) 310.

[44] A. Ringwald and F. Schrempp, DESY 94-197, DESY 96-125;
S. Moch, A. Ringwald and F. Schrempp, DESY 96-202;
M. Gibbs, A. Ringwald and F. Schrempp, DESY 95-119.

[45] H1 Collab., S. Aid et al., DESY 96-122.

[46] M. Gibbs et al., contrib. to the workshop on "Future Physics at HERA", Hamburg 1995-1996.

[47] H1 Collab., T. Ahmed et al., Phys. Lett. B346 (1995) 415.

[48] ZEUS Collab., M. Derrick et al., Phys. Lett. B363 (1995) 201.

[49] T. Brodkorb and E. Mirkes, MADPH-94-821 .

[50] H.U. Martyn, Proc. of the DIS96 workshop, Rome 1996;
H1 Collab., contrib. paper pa02-076 to ICHEP'96, Warsaw 1996.

[51] B. Webber, appeared in the Proc. of the Workshop on Deep Inelastic Scattering and QCD - DIS95, Paris, April 1995, eds. JF. Laporte and Y. Sirois, p. 345.

[52] ZEUS Collab., contrib. paper pa02-034 to ICHEP96, Warsaw 1996.

[53] D. Graudenz, CERN-TH/96-155, CERN-TH/96-187.